

Enhanced adsorption of chromium(VI) from aqueous medium by basic nanohydroxyapatite/chitosan composite based on egg shell

Asaad F. Hassan^{a,*}, Gehan A. El-Naggar^a, Amany G. Braish^a, Mohamed F. Amira^b,
Laila M. Alshandoudi^c

^aChemistry Department, Faculty of Science, Damanshour University, Damanshour, Egypt, emails: asmz68@sci.dmu.edu.eg/
asmz68@yahoo.com (A.F. Hassan), gica7000@yahoo.com (G.A. El-Naggar), amany.braish@yahoo.com (A.G. Braish)

^bChemistry Department, Faculty of Science, Alexandria University, Alexandria, Egypt, email: mohamed.f.amira@gmail.com (M.F. Amira)

^cScience Department, Rustaq College of Education, Directorate of General Applied Science, Rustaq, Sultanate of Oman,
email: lailaj.rus@cas.edu.om (L.M. Alshandoudi)

Received 16 February 2020; Accepted 27 June 2020

ABSTRACT

Four solid adsorbents namely nanohydroxyapatite (NP), cetyltrimethyl ammonium bromide modified nanohydroxyapatite (NPB), and nanohydroxyapatite/chitosan composite either in acidic (NPS₁) or basic media (NPS₂) were prepared based on egg shell as a biosource. Solid materials were characterized by N₂ adsorption/desorption isotherms, scanning electron microscopy, X-ray diffraction, transmission electron microscopy, Fourier transform infrared spectroscopy, and point of zero charges. The thermal, textural, and chemical properties of nanohydroxyapatite/chitosan composite prepared in basic medium were found to be more enhanced than the other three solid adsorbents with surface area and pore radius of 152.5 m²/g and 5.11 nm, respectively. pH_{PZC} for all the prepared solid samples ranged between 6.8 and 7.5. Adsorption of hexavalent chromium were studied under different application condition such as the effect of adsorbent dosage, time, pH, initial Cr(VI) concentration, and temperature. The maximum adsorption capacities of chromium onto NP, NPS₁, NPS₂, and NPB (119.047, 131.578, 134.048, and 85.397 mg/g, respectively) were observed at pH 6. Thermodynamic and kinetic parameters proved that adsorption of Cr(VI) onto all the investigated solid adsorbents follow pseudo-second-order kinetic model, spontaneous, and endothermic adsorption process.

Keywords: Egg shell; Nanhydroxyapatite; Chitosan; Chromium; Adsorption; Kinetics; Thermodynamics

1. Introduction

Water pollution caused by toxic heavy metal ions from different anthropogenic and natural sources has become one of the most dangerous problems in recent years, due to their natural resistance to degradation and high toxicity even at trace concentrations [1–3]. Heavy metal contamination exists in aqueous waste streams of many industries and agricultural activities which may pose a serious threat to the environment [4,5]. Heavy metals are common in industrial

applications such as in the manufacture of alloys, batteries, pesticides, electroplated metal parts, steel, dyes, mining, fertilizers manufactures, refining ores, electronic industries, petrochemical processes, paper industries, and tanneries [6]. Hexavalent chromium is considered as one of the most known heavy metals that have been a major focus in wastewater and water treatment [7]. Chromium is addressed as the 20th first most abundant elements in the earth crust [8]. Chromium can exist in valences from 2+ to 6+, but is present in the environment mainly in the stable form of Cr³⁺ and Cr⁶⁺

* Corresponding author.

[9]. The chemical properties and toxicity of Cr^{6+} is mainly depends on the differences in its oxidation state [10]. Due to the carcinogenic and tetragenic characteristics of Cr^{6+} , many researchers consider it as one of the top sixteen toxic pollutants. World Health Organization (WHO) specifying its tolerance limit as 0.05 mg/L. Hexavalent chromium is a mutagenic and carcinogenic to all living cells due to the DNA modification and causing important chromosomal aberrations and can also cause skin rashes, lung cancer, ulcers, and upset stomachs, weakened immune systems, respiratory problems, as well as kidney, gastric, and liver damage [11]. Chromium passed to the environment through industrial operations such as metal finishing industry, steel and chromium industries, pigment manufacturing and paint, corrosion control, chrome plating, leather tanning, fertilizer, and wood preservation, textile production, inorganic chemical production, and photography [12].

Methods which were used to remove pollutants include filtration, precipitation, coagulation, magnetic fields, ion exchange, ion flotation, fluidized bed reactor, chemical oxidation, reduction, solvent extraction, electrolytic recovery, reverse osmosis, evaporation, flue gas purification, and biological methods [13–17]. Adsorption technique has been found to be superior as related to the other methods for water reuse in terms of flexibility, initial cost, and simplicity of design, insensitivity to toxic pollutants, ease of operation, solid adsorbents reusability, and not leads to toxic products [18,19].

In recent years, nanomaterials like biological origin like chitin and hydroxyapatite, chitosan, lignin is one of the new developed solid adsorbents to remove toxic inorganic and organic pollutants [20]. Apatite with the general chemical formula of $M_{10}(X)_6(Y)_2$, herein M represents divalent cations (Mg^{2+} , Ca^{2+}), X is related to di or trivalent anions (CO_3^{2-} , PO_4^{3-}), and Y is monovalent anions (OH^- , Cl^- , and F^-) are the most identified natural phosphate minerals [21]. A crystal chemical analog of the bone tissue mineral component, teeth, and phosphate mineral rocks is hydroxyapatite ($\text{Ca}_{10}(\text{PO}_4)_6(\text{OH})_2$) [22]. The crystallographic structure of hydroxyapatite are arranged in a hexagonal shape and formed by a hexagonal stack of isolated phosphate ion tetrahedrons which is responsible for creation of tunnels [23]. Calcium ions on hydroxyapatite surface could exchange heavy metals such as Cu^{2+} , Cd^{2+} , Hg^+ , Zn^{2+} , Cr^{6+} , Pb^{+2} , etc. [24,25]. Hydroxyapatite is characterized by obvious properties of biocompatibility, bioactivity, nontoxicity, non-inflammatory, and non-immunogenicity [26]. Pure hydroxyapatite is stable up to 1,200°C [27] and considered as an ideal solid adsorbent for the removal of contaminants due to its higher adsorption capacity, low solubility in water (K_{sp} less than 10^{-40}), high stability under heating and redox conditions, low cost, and availability [28]. It can behave as both cation and anion exchange media [29]. Synthesis processes might be either complicated or expensive. The recent production methods of hydroxyapatite based on natural sources have gained researchers attention [30]. Egg shells have been introduced as a promising source because egg shells easily procured [31]. Approximately 11% of the total weight of egg is egg shell with chemical composition of 94%, 1%, 1%, 4% calcium carbonate, magnesium carbonate, calcium phosphate, and organic matter, respectively [32]. Dried nanohydroxyapatite agglomeration is the

major challenge responsible for the reduction in its surface area and adsorption capacity and to obtain well-dispersed nanoparticles without agglomeration, surfactants must be introduced to the reaction mixture during the preparation process [33–35]. Chitin is formed of a linear chain of acetyl glucosamine while chitosan is produced by deacetylation process via the removal of chitin acetyl groups (CH-CO) using concentrated sodium hydroxide for long time period at elevated temperature. The presence of hydroxyl and amino groups on the surface of chitosan act as adsorption active sites. Pure nanohydroxyapatite is not suitable for the adsorption of anionic pollutants from aqueous media thus surface chemical modification of the pure nanohydroxyapatite with chemical agent is essential to reach suitable surface charge to raise its adsorption efficiency [36–40].

The main objective of this research work is the preparation of nanohydroxyapatite (NP), nanohydroxyapatite/chitosan composite either in acidic (NPS_1) or basic (NPS_2) media, and cetyltrimethyl ammonium bromide modified nanohydroxyapatite (NPB). Full characterizations of the prepared solid adsorbents including thermal, textural, and chemical characterization will be investigated. Adsorption of chromium(VI) from aqueous solution by all the solid adsorbents will be carried out considering different application conditions, kinetic, and thermodynamic studies. Egg shells is a solid waste that will be converted into valuable nanohydroxyapatite as solid adsorbents for heavy metal cations adsorption after surface modification. All solid adsorbents are easily renewable using diluted nitric acid as a desorbing solution.

2. Materials and methods

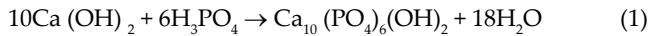
2.1. Materials

Potassium dichromate ($\geq 99.5\%$), orthophosphoric acid (85 wt.%), chitosan (85% deacetylated), acetic acid (99.5%), sodium hydroxide (98%), cetyltrimethyl ammonium bromide (CTAB, $\geq 99\%$), and ethanol (95%) were supplied by Sigma-Aldrich, (St. Louis, MO, USA). Stock solution of each compound was prepared using deionized water.

2.2. Preparation of solid adsorbents

2.2.1. Preparation of nanohydroxyapatite (NP)

Hydroxyapatite nanoparticles were prepared using egg shells as a bio natural source of calcium [41,42]. Egg shells were collected from local restaurant and cleaned manually by distilled water. After drying, they were ground in a mortar and dried in oven for 3 h at 110°C followed by calcination in a muffle furnace for 6 h at 900°C to obtain calcium oxide powder. CaO (4 g) was mixed with 700 mL of distilled water and stirring vigorously by using a heating magnetic stirrer at 50°C for 2 h. Calcium oxide was converted into $\text{Ca}(\text{OH})_2$ after dispersing in distilled water. Under vigorous stirring, 0.4 M H_3PO_4 was added drop by drop with a constant rate to the suspension at room temperature. Initially, the pH of the solution was measured to be 10.5 but at the end of orthophosphoric acid addition, it decreases to 7.5. After orthophosphoric acid was completely added, precipitate was formed and the formed precipitate was subjected to aging for 24 h. The expected reaction is as follows:



The precipitate was separated by filtration, washed with distilled water, dried at 100°C for 4 h, and calcined at 900°C for 4 h (NP).

2.2.2. Preparation of nanohydroxyapatite/chitosan composite in acidic medium (NPS₁)

To prepare NP/chitosan composite in acidic medium, 1 g of chitosan was dissolved in 2% acetic acid solution (100 mL). One gram of NP was dispersed in 25 mL distilled water and completely transferred into the chitosan solution using a dropper. The solution was mechanically stirred for 24 h to disperse the NP particles in the polymer matrix homogeneously. The solution was carefully filtered and dried at 90°C (NPS₁).

2.2.3. Preparation of nanohydroxyapatite/chitosan composite in basic medium (NPS₂)

One gram of chitosan powder was dissolved in 2% acetic acid solution (100 mL). To the last solution we added NP (1.0 g) and stirring for 60 min till homogenous solution. By syringe, the suspension was dropped into 20 mL 3.0% (w/v) aqueous solution of NaOH. After 24 h the formed beads were filtered and washed with distilled water for several times, followed by 3 mL 95% ethanol and distilled water as mixed washing solution. The produced composite was dried at 90°C for 24 h (NPS₂).

2.2.4. Preparation of cetyltrimethyl ammonium bromide modified nanohydroxyapatite (NPB)

Cetyltrimethyl ammonium bromide modified nanohydroxyapatite was prepared by intercalation method as reported by Mehdi et al. [36]. Two grams of NP were dispersed using a magnetic stirrer in 100 mL of distilled water for 24 h at room temperature. CTAB (1.0 g) was slowly added to the previous mixture. The reaction mixture was stirred for 5 h, filtered, washed several times with distilled water, and dried at 90°C for 24 h (NPB).

2.3. Characterization of the prepared solid adsorbents

Thermal stability of egg shell, NP, NPB, NPS₁, and NPS₂ was investigated using differential thermal analyzer Shimadzu DTA-50, Japan in nitrogen atmosphere with heating rate of 15°C/min up to 800°C.

The weight loss during drying was calculated for all samples by weighing 0.5 g of the sample in crucible and put it in the oven for 24 h at 110°C until the weight of the sample reaches constant weight.

$$\text{Weight loss on drying (\%)} = \frac{W_b - W_a}{W_b} \times 100 \quad (2)$$

where W_b and W_a are the weight of sample before and after drying.

The textural structure of the samples was examined by using SEM Quanta 250 FEG, Japan. The morphology of the

prepared adsorbent particles was also studied using transmission electron microscopy (TEM), Technai 20 (Philips, Holland).

The specific surface area S_{BET} (m²/g), average pore radius \bar{r} (nm), and total pore volume V_p (mL/g) were determined by N₂ adsorption according to Brunauer–Emmett–Teller (BET) method at –196°C using NOVA 2000 gas sorption analyzer (Quantachrome Corporation, USA).

Fourier transform infrared spectra (FTIR) were investigated for all the solid samples in the range 400–4,000 cm^{–1} using Mattson 5000 FTIR spectrometer, USA.

Point of zero charge (pH_{PZC}) was determined by; initially, 40 mL of 0.01 M NaCl were placed into closed Erlenmeyer flasks. The pH within each flask was adjusted in the pH range of 2–12 by adding either HCl (0.02 M) and/or NaOH (0.02 M). Then, a portion of the adsorbent sample (0.15 g) was added to each flask, the flasks were shaken for 48 h, and the final pH was then measured. The pH_{PZC} is the point at which pH_{final} – pH_{initial} = zero [43].

2.4. Adsorption of Cr⁶⁺ from aqueous medium

Aqueous solution with definite concentration of Cr⁶⁺ (50–300 mg/L) was shaken in Pyrex bottles of 50 mL capacity containing 0.05 g of solid adsorbent (NP, NPS₁, NPS₂, or NPB) for 24 h and the supernatant liquid was filtered out. The liquid equilibrium concentration of Cr⁶⁺ (C_e or C_t mg/L) was determined by the atomic absorption spectrometer (Sens AA, USA) at 357.9 nm. The adsorbed amount at equilibrium, q_e (mg/g) was calculated by the following equation.

$$q_e = \frac{C_0 - C_e}{m} \times V \quad (3)$$

where C_0 and C_e are the initial and final concentration of Cr⁶⁺ (mg/L). V is the volume of Cr⁶⁺ solution (L), and m is the mass of adsorbents (g). The effect of time (10–100 min) and pH (2–8) were carried out by shaking 0.05 g of adsorbents with 50 mL of Cr⁶⁺ solutions of known concentration (100 mg/L). Adsorption capacity (q_t) after recorded time intervals was calculated using Eq. (4):

$$q_t = \frac{(C_0 - C_t)V}{m} \quad (4)$$

where C_t is the concentration of Cr⁶⁺ in solution at time t (mg/L).

2.5. Solid adsorbent reusability

Desorption study was investigated by weighting 0.5 g of NPS₂ and mixed with 200 mL of 300 mg/L Cr⁶⁺ ion solution and shaken for 60 min at room temperature. The solid sample was filtered off and washed with distilled water, dried, and mixed with 50 mL of desorbing solution (distilled water, 0.05 M nitric acid, or 0.05 M hydrochloric acid) for 3 h. Filter and determine the concentration of Cr⁶⁺ in the filtrate. The desorption ratio was calculated using the following equation [44]:

$$\text{Desorption ratio} = \frac{\text{Amount of chromium (IV) ions desorbed}}{\text{Amount of chromium (VI) ions adsorbed}} \times 100 \quad (5)$$

The reusability of NPS₂ was investigated after four cycles of chromium adsorption/desorption. After each cycle, NPS₂ was filtered and mixed with hot HNO₃ (40 mL, 0.05 M) to desorb Cr⁶⁺ ions, washed with hot water, dried, and used in the successive cycle.

3. Results and discussion

3.1. Thermal characterization

NP exhibited the smallest % of weight loss on drying compared with the other prepared solid adsorbents and loss in drying increases with modification of NP either with chitosan or CTAB (Table 1). The higher loss on drying for NPS₂ (3.2%) is related to the increase in surface modification which raises the polar surface functional groups beside the increase in the surface area as determined by FTIR and nitrogen adsorption data, respectively. TGA for egg shells, NP, NPS₁, NPS₂, and NPB are shown in Fig. 1. Egg shell showed weight loss about 7% below 180°C and may be related to the physically adsorbed water. Egg shells showed a weight loss of about 18% in the range 200°C–450°C which is due to the oxidation of organic contents in the egg shell [45]. Then calcination of egg shell started at about 650°C till 770°C. At this range nearly all CaCO₃ decomposes into CaO with the evolution of CO₂ (Eq. (6)) [46]. NP showed 3% weight loss in the range 400°C–800°C which can be related to water loss from HPO₄²⁻ and CO₃²⁻ decomposition on calcination at 800°C to form calcium oxide [Eqs. (7) and (8)] [47,48].



The mass loss of organic modified nanohydroxyapatite (NPB) is more than loss in case of unmodified sample (NP) due to the thermal decomposition of CTAB as organic compounds. Nanohydroxyapatite/chitosan composites showed 7% and 3% weight loss for NPS₁ and NPS₂, respectively, in the range 230°C–500°C which may be related to the decomposition of chitosan as well as the volatile substance evolved

from the inorganic compound decomposition [49]. At temperature above 600°C, there is no observable mass loss detected due to the formation of ash. This result indicates that chitosan was not simply adhered on NP surface, but completely mixed with NP to form composites.

3.2. Textural characterization of solid adsorbents

Surface area (S_{BET} , m²/g), total pore volume (V_p , cm³/g), and pore radius (\bar{r} , nm) for NP, NPB, NPS₁, and NPS₂ are listed in Table 1. NP has the highest surface area among NPB and NPS₁ because of the higher percentage of small particle size. NPS₁ has the lowest surface area because it has a larger particle size as indicated by TEM observations, and may be related to blocking of pores by chitosan molecules. For NPS₂, the formation of composite in the presence of NaOH₂ increases the surface area and total pore volume (0.389 cm³/g) which can be related to the porous nature of chitosan pellets.

The average pore radius in nm can be determined from the following equation:

$$\bar{r} \text{ (nm)} = \frac{2V_p \text{ (mL/g)}}{S_{\text{BET}} \text{ (m}^2\text{/g)}} \times 10^3 \quad (9)$$

where V_p defined as the volume of liquid nitrogen expressed in (cm³/g), at relative pressure approaching unity

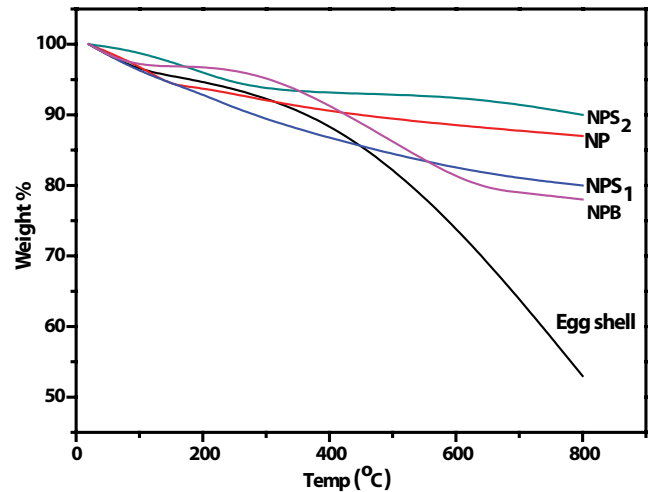


Fig. 1. TGA of egg shell, NP, NPB, NPS₁, and NPS₂ as solid adsorbent samples.

Table 1

Loss on drying, pH_{pzc} and textural parameters derived from nitrogen adsorption at -196°C onto NP, NPB, NPS₁, and NPS₂

Sample	Weight loss on drying (%)	pH _{pzc}	S_{BET} (m ² /g)	V_p (cm ³ /g)	\bar{r} (nm)
NP	1.2	6.8	103.7	0.188	3.63
NPB	1.8	6.9	98.6	0.150	3.06
NPS ₁	2.8	7.3	91.5	0.233	5.10
NPS ₂	3.2	7.5	152.5	0.389	5.11

at $P/P^0 = 0.95$. It was found that the average pore radius for all sample in the range 3.06–5.11 indicating the mesoporous range formed due to aggregation of nanoparticles.

SEM images are shown in Figs. 2a–d where NP powders are presented as particles but in the case of NPS_1 and NPS_2 composites appeared as larger aggregates which confirmed the formation of hydroxyapatite/chitosan composites. In the case of NPB, the crystal structure of NP powder surfaces were fully covered with respective CTAB. The previous observation confirms that the material showed a suitable surface morphology for Cr^{6+} adsorption.

TEM micrographs of the prepared samples are displayed in Figs. 3a–d. These micrographs indicate nanometer scale size of samples particles. The comparison of the relative micrographs of figures reveals some significant changes between morphology and size of the particles. From the histogram of TEM (Fig. 3e), we observed that the size of the NP and NPB in the range of 30–50, 50–150 nm, while for NPS_1 and NPS_2 located in the range of 150–200 nm, respectively. Chitosan could have possibly accelerated NP crystal nuclear growth; henceforth increasing the particle size of NP in the presence of chitosan [49].

It is known that beside the physical structure, the solid adsorbents have a chemical structure that also affects as well

on the adsorption capacity. Infrared spectroscopy has been one of the most frequently used techniques to characterize the surface functionalities in nanohydroxyapatite and other solid adsorbents. FTIR spectra for NP, NPB, NPS_1 , and NPS_2 are shown in Figs. S1a–d respectively. In Fig. S1a, the band at 632; 3,500–3,200 cm^{-1} and 1,636; 3,446 cm^{-1} are related to stretching vibrations and bending of the hydroxyl groups, respectively, present in NP [50]. The band at 560–610 and 1,000–1,100 cm^{-1} in NP related to PO_4^{3-} stretching vibrations and bending, respectively [51,52]. In Fig. S1b, the observed band around 3,572 cm^{-1} corresponding to the stretching vibration of the –OH group and the interlayer water molecules was observed. In Figs. S1c and d, the –NH group of chitosan is observed at 1,634 cm^{-1} . The stretching and bending vibration mode of –NH group of chitosan occurred at 3,452 and 1,627 cm^{-1} , respectively which was overlapped with the bands of O–H groups in composite [53]. The vibration bands of C–O group are overlapped with phosphate bands at 1,150–1,046 cm^{-1} . The FTIR spectra of NPS_1 and NPS_2 showed a band at 1,032 cm^{-1} which was due to stretching vibration of C–O–C group of chitosan confirms the composite formation. In the FTIR spectra of NPS_1 and NPS_2 composites, the adsorption peaks proved that the chemical composition of NP did not change after integration.

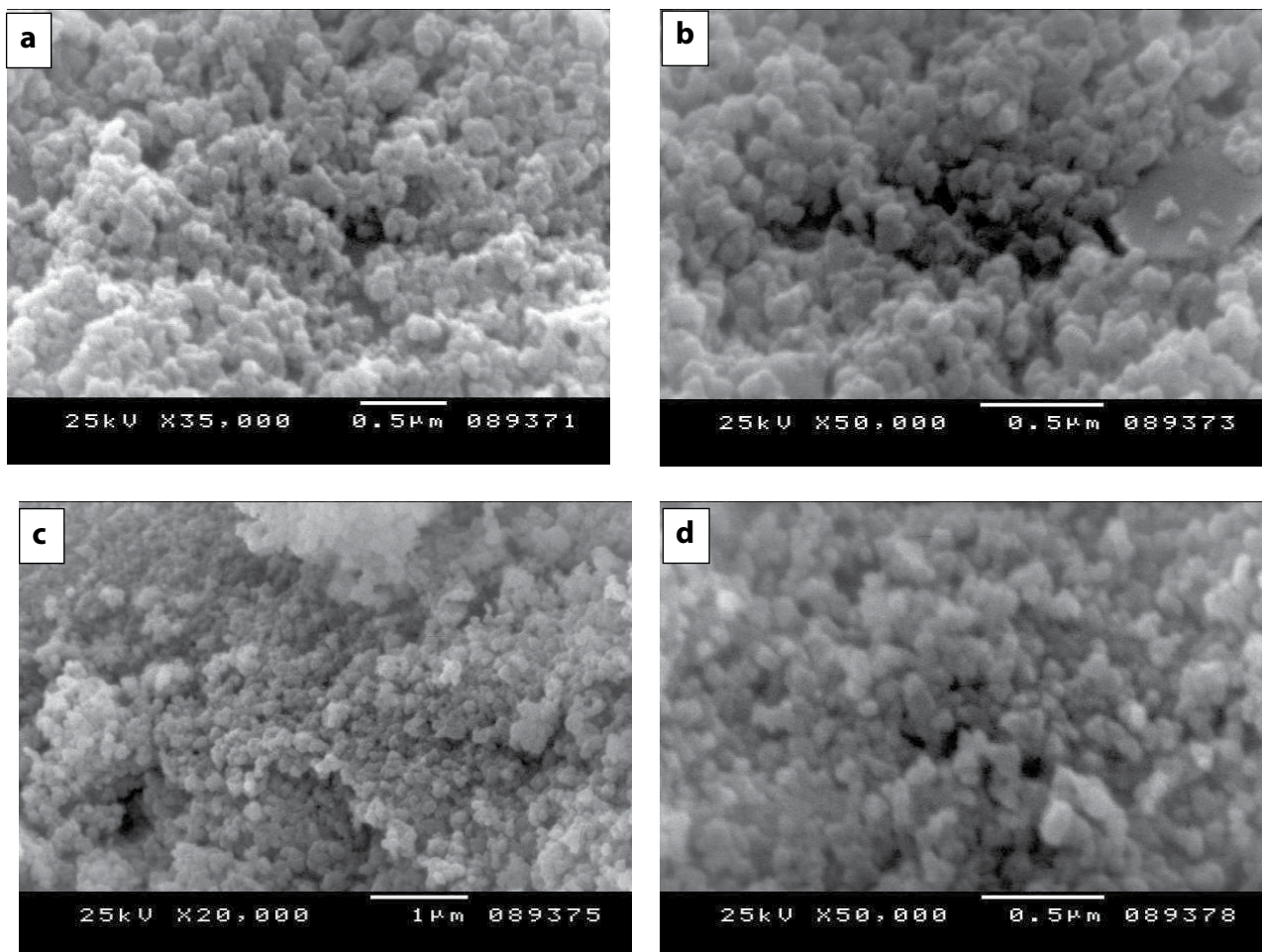


Fig. 2. SEM images of NP (a), NPB (b), NPS_1 (c), and NPS_2 (d), respectively.

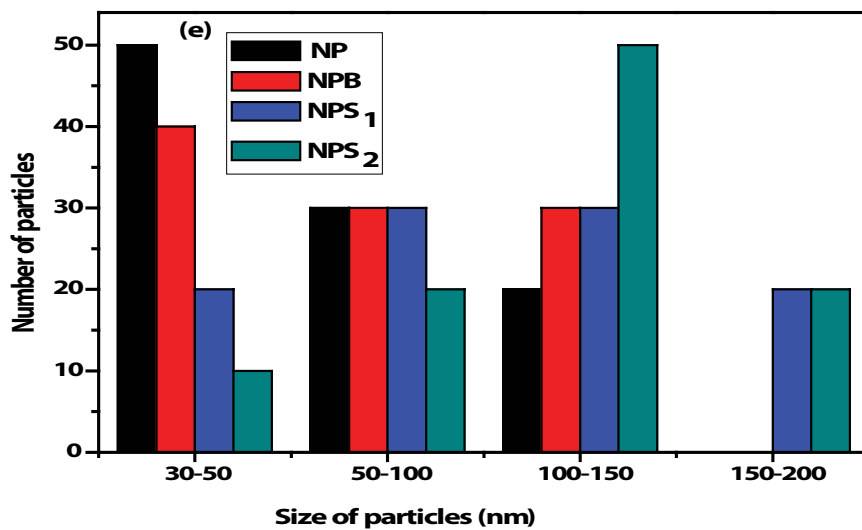
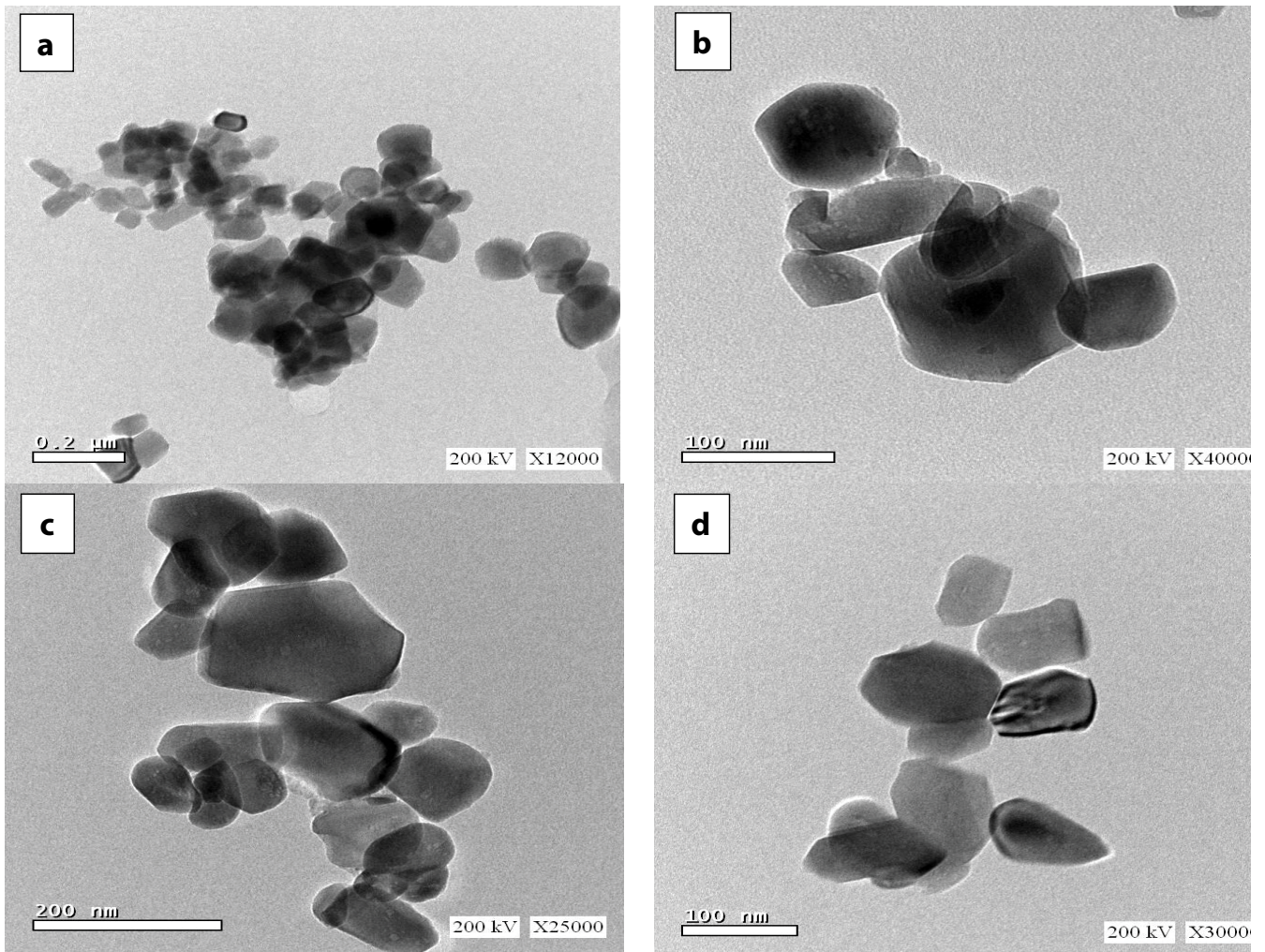


Fig. 3. TEM micrographs (a–d), and histogram (e) for NP, NPB, NPS₁, and NPS₂ respectively.

However, the strength of feature peaks of NP shifted to a lower wave number at different levels. This might be due to hydrogen bonding interaction occurring between OH^- in NP and $-\text{NH}_2$ in chitosan or the chelation between $-\text{NH}_2$ and calcium or NP particles occluded in the structure of chitosan to break the chains hydrogen bonding interaction [54].

The point of zero charge (pH_{pzc}) is important factor in the adsorption of cations from aqueous medium [55,56]. The pH_{pzc} of NP, NPB, NPS_1 , and NPS_2 are shown in Table 1. The pH_{pzc} of NP, NPB, NPS_1 , and NPS_2 were found to be 6.8, 6.9, 7.3, and 7.5, respectively. It was noted that at pH less than pH_{pzc} the surface of the adsorbent is predominated by positive charges while at pH more than pH_{pzc} the surface of the adsorbent is predominated by negative charges. This, in fact, anticipates a different adsorption efficiency for Cr^{6+} ions in solutions of different pH, and presumably, at lower pH values (the adsorbents are positively charged), the cation exchange mechanism will predominate, while at elevated pH values (the adsorbents are negatively charged), the controlling force for Cr^{6+} pollutants removal will be the electrostatic attractions [57]. The different pH_{pzc} values for NP, NPB, NPS_1 , and NPS_2 further confirm the composite formation.

3.3. Adsorption of chromium(VI) ions

3.3.1. Effect of pH

pH influences adsorption process of ions from their aqueous solution as it determines the magnitude and charge on ions beside its effects on the active sites quantity. The influence of pH on the adsorption process of Cr^{6+} ions onto NP, NPS_1 , NPS_2 , and NPB was studied as shown in Fig. 4a. The maximum adsorption of chromium occurs at pH 6, where removal efficiency reaches 52%, 67%, 70%, and 48% for Cr^{6+} onto NP, NPS_1 , NPS_2 , and NPB, respectively. In case of NP, NPS_1 , NPS_2 , and NPB, the removal efficiency for chromium ions at lower pH values is very low due to the presence of chromium as uncharged H_2CrO_4 with lower adsorption ability and the effect of H^+ ions which can exclude a significant number of active adsorption sites at NP, NPS_1 , NPS_2 , and NPB from the Cr^{6+} adsorption process

[58]. The uptake increased as pH values increased from 2 to 6 which can be related to the disappearance of H^+ ions competition and the presence of chromium oxyanions (HCrO_4^- or $\text{Cr}_2\text{O}_7^{2-}$) which can easily attracted to the free binding sites on the adsorbent surface [59]. At high pH values ($\text{pH} > 6$), OH^- may be attracted to the surface of the solid adsorbents through a hydrogen bond which contributes to the negatively charge sites of the solid adsorbents, and there would be a repulsion between these sites and the negatively charged chromium species (CrO_4^{2-}). Hence, it results in slowdown in the adsorbed amount of Cr^{6+} . pH 6 is the optimum suitable adsorption pH value for adsorption of Cr^{6+} onto the prepared solid samples.

3.3.2. Effect of adsorbent dosage

Adsorbent dosage relates to the ratio between the quantity of adsorbent active sites and adsorbate species. Fig. 4b shows the relationship between removal percent of Cr^{6+} against the adsorbent dosage (g/L). The removal percent was found to increase from 5%, 15%, 22%, 10% to 35%, 60%, 75%, and 40% with an increase in the adsorbent dosage of NP, NPS_1 , NPS_2 , and NPB from 1.0 to 6.0 g/L, respectively. As shown in Fig. 4b with the increase in adsorbent dosage, percentage removal of Cr^{6+} was also increased due to the increase in the number of active sites available for Cr^{6+} removal and the increase in surface area of adsorbents [60]. Increasing the adsorbent dosage (>6.0 g/L) leads to a slight increase in the removal efficiency which may be related to the attained equilibrium and the decrease in Cr^{6+} in relation to the available active sites on the solid adsorbent surface. The previous study indicates that 6.0 g/L is the most suitable adsorbent dosage for Cr^{6+} removals on the surface of the prepared solid adsorbents.

3.3.3. Effect of contact time and adsorption kinetics

Kinetic study provides information about the adsorption mechanism; it describes the rate of Cr^{6+} uptakes onto NP, NPB, NPS_1 , and NPS_2 against the adsorption time. The effects of contact time on the adsorption of Cr^{6+} onto

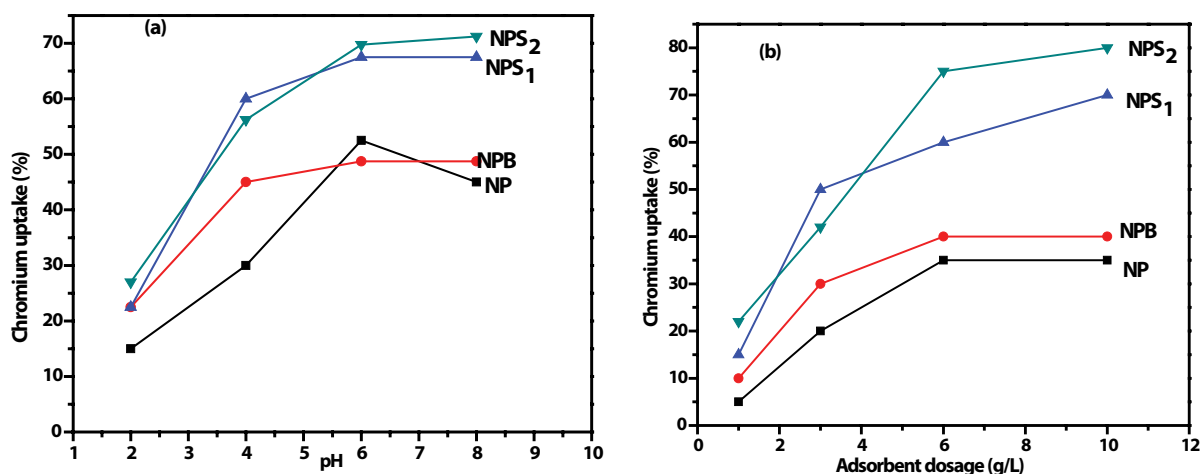


Fig. 4. Effect of pH (a) and adsorbent dosage (b) on the adsorption of chromium(VI) onto NP, NPB, NPS_1 , and NPS_2 at 20°C.

NP, NPB, NPS₁, and NPS₂ are shown in Fig. 5a. The amount of Cr⁶⁺ adsorbed q_t (mg/g) at time t , was calculated using Eq. (4). Fig. 5a shows that adsorption on the nanoadsorbents exhibited an initial rapid uptake followed by a slower removal rate that gradually reached equilibrium. The adsorption capacity of Cr⁶⁺ for NP, NPB, NPS₁, and NPS₂ at 0.2 h, in the range of (20–40 mg/g) and increased sharply at 0.8 h to 50, 60, 92, and 90 mg/g, respectively, which is related to the presence of abundant active binding sites available on the sorbents surface [61]. From the previous experiment, 1.0 h was selected as the equilibrium adsorption time for the adsorption of Cr⁶⁺ onto all nanoadsorbents.

Pseudo-first-order (PFO, Eq. 10) and pseudo-second-order (PSO, Eq.11) kinetic models were applied to express the mechanism of Cr⁶⁺ adsorption onto all the solid adsorbents.

$$\log(q_e - q_t) = \log q_e - \frac{k_1 t}{2.303} \quad (10)$$

$$\frac{t}{q_t} = \frac{1}{k_2 q_e^2} + \frac{t}{q_e} \quad (11)$$

where k_1 is the PFO adsorption rate constant (1/h) and t is the time (h) while k_2 is the PSO adsorption rate constant (g/mg h). Values of k_1 were calculated from the plots of $\log(q_e - q_t)$ vs. t as shown in Figs. 5b and c. PFO kinetic parameters indicates that adsorption of chromium onto adsorbents does not follow PFO due to the large difference between the calculated q_e (mg/g) from PFO model and that calculated from Langmuir adsorption model q_{\max} (mg/g) as listed in Table 2. Figs. 5d and e exhibited PSO kinetic model plots and the calculated PSO characteristics model parameters are shown in Table 2. Correlation coefficient (R^2) for the pseudo-second-order equation is slightly higher than that for the pseudo-first-order equation; this indicates that the adsorption process might be chemisorption [62,63]. Adsorption capacity values calculated from PSO model are nearly close to those estimated from Langmuir equation indicating the good applicability of PSO mechanism for the adsorption of chromium(VI).

Moreover, the intraparticle diffusion model was applied which conclude that the removal is proportional to the contact time square root during the adsorption (Eq. (12)):

$$q_t = k_d t^{0.5} + C \quad (12)$$

where k_d is the intraparticle diffusion rate constant. Values of C give information related to the thickness of the boundary layer [64]. The plot of q_t vs. $t^{0.5}$ was presented in Figs. S2a and b and showed that all the plots not passed through the origin indicating that the intraparticle diffusion was a part of the adsorption and it is not the rate-determining step. The multi-linearity through the whole range of time and prove that intraparticle diffusion was not the only rate-limiting mechanism [65]. The intraparticle diffusion model listed in Table 2 indicates the good applicability of Eq. (11) based on the higher correlation coefficients values (R^2 , 0.982–0.999).

3.3.4. Adsorption isotherm

Adsorption isotherms describe the relationship between the adsorbed amount and residual adsorbate concentration in the adsorption solution. The adsorption isotherm of chromium(VI) was studied on the samples prepared at 20°C and are presented in Fig. 6a. Langmuir and Freundlich isotherms have been tested as linear adsorption models. The linear form of Langmuir equation [Eq. (13)]:

$$\frac{C_e}{q_e} = \frac{1}{q_m b} + \frac{C_e}{q_m} \quad (13)$$

where q_m is the maximum adsorption capacity and b is known as the adsorption constant of Langmuir model. Langmuir isotherm parameters q_m and b were calculated from the respective slope and intercept of the linear plot of C_e/q_e vs. C_e as shown in Figs. 6b and c and parameters are displayed in Table 3. Upon inspection of Table 3 (i) NPS₂ and NPS₁ have the maximum adsorption capacity and may be attributed to the presence of chitosan functional groups, which is able to bind Cr⁶⁺ ions. (ii) Linear Langmuir correlation coefficient values (R^2) ranged between 0.937 and 0.999 indicates the good applicability of Langmuir adsorption model. R_L (dimensionless separation factor) is defined as:

$$R_L = \frac{1}{(1 + bC_0)} \quad (14)$$

If $R_L > 1$ the adsorption is unfavorable, if $0 < R_L < 1$ the adsorption is favorable, and reversible adsorption in the case of $R_L = 0$. R_L values for chromium(VI) adsorption onto NP, NPB, NPS₁, and NPS₂ were less than unite and more than zero (0.12–0.35) indicating favorable adsorption of Cr⁶⁺ onto all the solid adsorbents.

Table 2

Kinetic model parameters (pseudo-first-order and pseudo-second-order) and intraparticle diffusion parameters for adsorption of chromium(VI) onto NP, NPB, NPS₁, and NPS₂ at 20°C

Adsorbents	q_{\max} (mg/g)	Pseudo-first-order kinetic model			Pseudo-second-order kinetic model			Intraparticle diffusion parameters		
		q_e (mg/g)	k_1 (1/h)	R^2	q_e (mg/g)	k_2 (g/mg h)	R^2	k_d (mg/g h ^{0.5})	C	R^2
NP	119.047	63.509	1.442	0.9180	115.300	0.012	0.9478	84.808	22.272	0.999
NPB	85.397	40.305	0.943	0.9010	83.942	0.053	0.9994	58.095	10.134	0.991
NPS ₁	131.578	100.524	2.330	0.9271	135.888	0.014	0.9591	148.600	36.021	0.982
NPS ₂	134.048	198.864	2.872	0.9292	142.366	0.005	0.9592	131.347	33.432	0.999

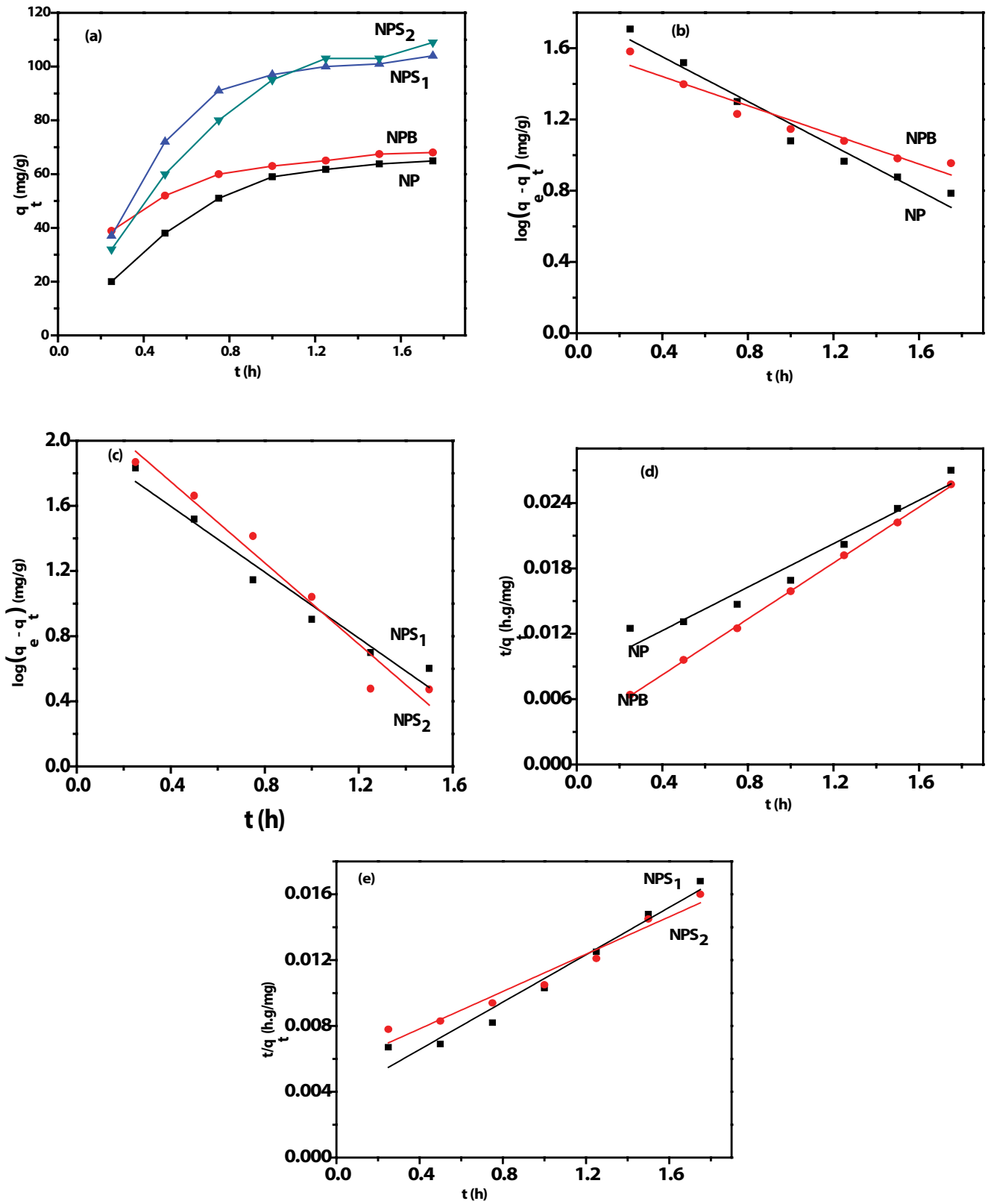


Fig. 5. Effect of contact time (a), pseudo-first (b and c), and pseudo-second-kinetic-order (d and e) models for adsorption of chromium(VI) onto NP, NPB, NPS₁, and NPS₂ at 20°C.

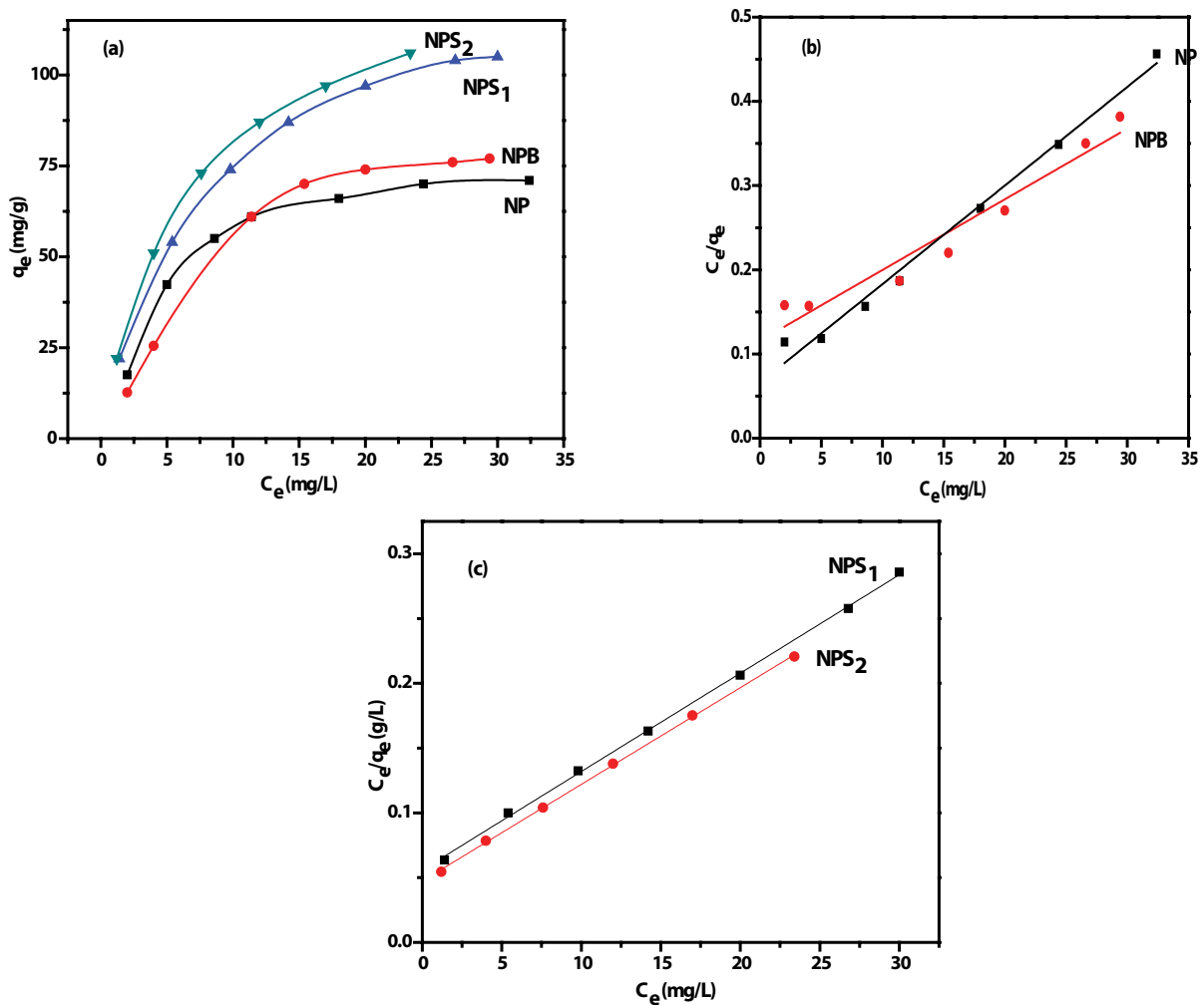


Fig. 6. Adsorption isotherm (a) and linear Langmuir plot (b and c) for chromium(VI) adsorption on NP, NPB, NPS₁, and NPS₂ at 20°C.

Table 3

Langmuir and Freundlich adsorption isotherm parameters for chromium(VI) adsorption onto NP, NPB, NPS₁, and NPS₂ at 20°C

Adsorbents	Langmuir parameters				Freundlich parameters		
	q_{\max} (mg/g)	b (L/mg)	R^2	R_L	K_F	$1/n$	R^2
NP	119.047	0.072	0.937	0.12	16.341	0.479	0.937
NPB	85.397	0.177	0.987	0.13	9.321	0.680	0.936
NPS ₁	131.578	0.135	0.999	0.24	20.701	0.512	0.963
NPS ₂	134.048	0.157	0.999	0.35	22.181	0.532	0.965

Freundlich isotherm is interested in multilayer adsorption and interaction between adsorbed molecules. Freundlich model applies to the adsorption on solid surfaces with heterogeneous nature with reversible adsorption [45].

The Freundlich isotherm is represented by:

$$q_e = K_F C_e^{1/n} \quad (15)$$

Here K_F and n are known as Freundlich adsorption capacity and Freundlich constant related to the adsorption

intensity, respectively. The Freundlich equation is expressed linearly as:

$$\ln q_e = \ln K_F + \frac{1}{n} \ln C_e \quad (16)$$

The values of Freundlich isotherm constants for the sorbents were calculated from the linear plot of $\ln q_e$ against $\ln C_e$ as shown in Fig. S3 and parameters are presented in Table 3. Freundlich parameters from Table 3 predict that

$n > 1$ and illustrates the adsorption process is favorable on solid adsorbents [66]. Correlation coefficient (R^2) ranged between 0.936 and 0.965 indicates good applicability of the Freundlich adsorption model. $1/n$ values ranged between 0.479 and 0.680 for Cr^{6+} adsorption by all the prepared solid adsorbents (lower than unit) revealed that a normal Langmuir isotherm [67].

3.3.5. Comparison of NPS_2 with other solid adsorbents for hexavalent

In this study, NPS_2 was compared with other solid adsorbents (Table 4) [68–73]. The reported data in the Table represents the higher efficiency for nanohydroxyapatite/chitosan composite prepared in basic medium (NPS_2) as a promising solid adsorbent for heavy metal ions from an aqueous medium.

3.3.6. Effect of temperature and thermodynamic studies

In general, the temperature dependence is associated with three parameters of thermodynamic namely the change in enthalpy of adsorption (ΔH° , kJ/mol), change in entropy of adsorption (ΔS° , kJ/mol K), and change in Gibbs free energy (ΔG° , kJ/mol). Thermodynamic parameters of Cr^{6+} adsorption onto NPS_2 were determined at three different temperatures namely 20°C, 30°C, and 40°C as shown in Fig. S4a. The curve showed that the adsorption of Cr^{6+} increases with temperature indicating the endothermic nature for the adsorption of Pb^{2+} onto NSP_2 . The distribution coefficient was calculated as:

$$K = \frac{C_s}{C_e} \quad (17)$$

where C_s and C_e are the concentration of Cr^{6+} onto the adsorbent surface and the equilibrium concentration, respectively. According to thermodynamic, Gibbs free energy change is related to change in entropy of adsorption at constant temperature by Van't Hoff model [Eq. (18)]:

$$\ln K = \frac{\Delta S^\circ}{R} - \frac{\Delta H^\circ}{RT} \quad (18)$$

Table 4
Comparison between Langmuir maximum adsorption capacities of hexavalent chromium onto NPS_2 and other solid adsorbents

Adsorbents	q_m (mg/g)	References
CS-SSM	112.5	[68]
Chitosan nanofibers	70.0	[69]
Metal-organic framework	48.0	[70]
Amino-functionalized MIL-101(Cr)	44.0	[71]
Three-dimensional (3D) hierarchically porous NiO/Ni composites	73.00	[72]
SWNTs	4.9	[73]
NPS_2	134.1	(This study)

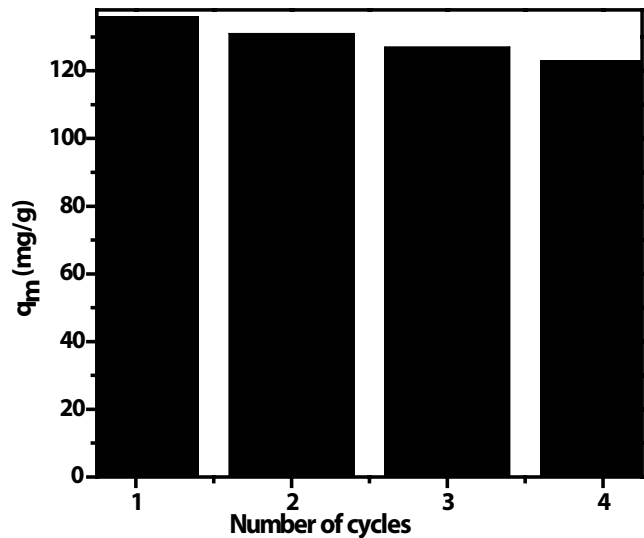


Fig. 7. Reusability of NBS_2 for hexavalent chromium adsorption after four cycles of adsorption/desorption at 20°C.

where R and T are the universal ideal gas constant (8.314 J/mol K) and the absolute adsorption temperature (K), respectively. Thus ΔH° and ΔS° can be calculated from the slope and intercept of the linear Van't Hoff plot ($\ln K$ against $1/T$) as shown in Fig. S4. The thermodynamic parameters, ΔS° and ΔH° were found to be 0.049 kJ/mol K and 8.600 kJ/mol, respectively. The negative values for ΔG° (−5.442, −5.949, and −6.373 kJ/mol) at 20°C, 30°C, and 40°C, respectively indicating the spontaneous nature of Cr^{6+} adsorption by all the adsorbents. The positive value of ΔS° proved that the freedom of Cr^{6+} ions is not much restricted in the adsorbent and increased the randomness at the solid/liquid interface during Cr^{6+} ions adsorption. Adsorption of Cr^{6+} onto all the solid adsorbents showed positive values for ΔH° which confirms the endothermic nature of the adsorption process.

3.4. Desorption and reusability of NPS_2

Desorption studies prove that nitric acid is the most suitable desorption solution where desorption ratio of $\text{HNO}_3 > \text{HCl} > \text{distilled water}$ (97%, 83%, and 59%, respectively). Reusability curve (Fig. 7) shows that solid adsorbent is a good reusable even after four cycles of adsorption and desorption. The decrease in adsorption capacity of solid adsorbent after four cycles (9.5%) due to the loss of some surface active sites as a result of solid adsorbent particle coagulation [74].

4. Conclusion

Four solid adsorbents namely; nanohydroxyapatite, nanohydroxyapatite CTAB, chitosan either in acidic or basic medium were prepared based on egg shell as a bio source for nanohydroxyapatite (NP, NPB, NPS_1 , and NPS_2 , respectively). Thermal stability experiments, chemical analysis, and textural characterization of the prepared solid adsorbents indicate the higher porosity, surface area, and total pore volume of nanohydroxyapatite/chitosan

composite prepared in basic medium (NPS₂). The adsorption of chromium(VI) onto NP, NPB, NPS₁, and NPS₂ was observed at pH = pH_{PZC}. NPS₂ predicted the higher adsorption capacity for Cr⁶⁺ (134.048 mg/g). The adsorption of chromium(VI) follows PSO kinetic model. Chromium(VI) adsorption onto solid adsorbents exhibited spontaneous and endothermic process as indicated by the thermodynamic parameters. Solid adsorbent is good reusable even after four cycles of adsorption and desorption with a small decrease in adsorption capacity. The results confirmed the promising adsorption nature of nanohydroxyapatite/chitosan composite as a new solid adsorbents for the environmental application.

References

- [1] A. Rashid, H.N. Bhatti, M. Iqbal, S. Noreen, Fungal biomass composite with bentonite efficiency for nickel and zinc adsorption: a mechanistic study, *Ecol. Eng.*, 91 (2016) 459–471.
- [2] K. Abida, N.B. Haq, M.K. Gillian, Re-use of agricultural wastes for the removal and recovery of Zr(IV) from aqueous solutions, *J. Taiwan Inst. Chem. Eng.*, 59 (2016) 330–340.
- [3] D. Vilela, J. Parmar, Y. Zeng, Y. Zhao, S. Sánchez, Graphene-based microbots for toxic heavy metal removal and recovery from water, *Nano Lett.*, 16 (2016) 2860–2866.
- [4] F. Fu, Q. Wang, Removal of heavy metal ions from wastewaters: a review, *J. Environ. Manage.*, 92 (2011) 407–418.
- [5] I. Mobasherpour, E. Salahi, M. Pazouki, Comparative of the removal of Pb²⁺, Cd²⁺ and Ni²⁺ by nanocrystallite hydroxyapatite from aqueous solutions: adsorption isotherm study, *Arabian J. Chem.*, 5 (2012) 439–446.
- [6] G. Fahimeh, M. Ahmad, E. Rahmatollah, Lead sorption properties of nanohydroxyapatite alginate composite adsorbents, *Chem. Eng. J.*, 200–202 (2012) 471–479.
- [7] G.N. Kousalya, M.G. Rajiv, S. Meenakshi, Removal of toxic Cr⁶⁺ ions from aqueous solution using nanohydroxyapatite based chitin and chitosan hybrid composites, *Adsorpt. Sci. Technol.*, 28 (2010) 49–64.
- [8] R.C. Saidur, K.Y. Ernest, Arsenic and chromium removal by mixed magnetite maghemite nanoparticles and the effect of phosphate on removal, *J. Environ. Manage.*, 91 (2010) 2238–2247.
- [9] S. Mor, K. Ravindra, N.R. Bishnoi, Adsorption of chromium from aqueous solution by activated alumina and activated charcoal, *Bioresour. Technol.*, 98 (2007) 954–957.
- [10] M. Abbas, M. Adil, S. Ehtisham-ul-Haque, B. Munir, M. Yameen, A. Ghaffar, G.A. Shar, M. Asif Tahir, M. Iqbal, Vibrio, Bioluminescence inhibition assay for ecotoxicity assessment: a review, *Sci. Total Environ.*, 626 (2018) 1295–1309.
- [11] M. Iqbal, *Vicia faba* bioassay for environmental toxicity monitoring: a review, *Chemosphere*, 144 (2016) 785–802.
- [12] L.V.A. Gurgel, J.C.G. de Melo, J.C. de Lena, F.L. Gil, Adsorption of chromium(VI) ion from aqueous solution by succinylated mercerized cellulose functionalized with quaternary ammonium groups, *Bioresour. Technol.*, 100 (2009) 3214–3220.
- [13] C. Liu, H. Xu, H. Li, L. Liu, L. Xu, Z. Ye, Efficient degradation of methylene blue dye by catalytic oxidation using the Na₈Nb₆O₁₉·13H₂O/H₂O₂ system, *Korean J. Chem. Eng.*, 28 (2011) 1126–1132.
- [14] M. Alaqarbeh, M. Shammout, A. Awwad, Nano platelets kaolinite for the adsorption of toxic metal ions in the environment, *Chem. Int.*, 6 (2020) 49–55.
- [15] A.M. Alasadi, F.I. Khaili, A.M. Awwad, Adsorption of Cu(II), Ni(II) and Zn(II) ions by nano kaolinite: thermodynamics and kinetics studies, *Chem. Int.*, 5 (2019) 2258–2268.
- [16] F. Minas, B.S. Chandravanshi, S. Leta, Chemical precipitation method for chromium removal and its recovery from tannery wastewater in Ethiopia, *Chem. Int.*, 3 (2017) 291–305.
- [17] C.P. Ukpaka, BTX degradation: the concept of microbial integration, *Chem. Int.*, 3 (2017) 8–18.
- [18] K.G. Mc, M.S. Otterburn, A.G. Sweeney, The removal of colour from effluent using various adsorbents—III. Silica: rate process, *Water Res.*, 14 (1980) 15–20.
- [19] D. Lijing, Z. Zhiliang, Q. Yanling, Z. Jianfu, Removal of lead from aqueous solution by hydroxyapatite/magnetite composite adsorbent, *Chem. Eng. J.*, 165 (2010) 827–834.
- [20] G.N. Kousalya, G.M. Rajiv, S.C. Sairam, S. Meenakshi, Synthesis of nanohydroxyapatite chitin/chitosan hybrid biocomposites for the removal of Fe³⁺, *Carbohydr. Polym.*, 82 (2010) 594–599.
- [21] C. Stötzel, F.A. Müller, F. Reinert, F. Niederdraenk, J.E. Barralet, U. Gbureck, Ion adsorption behaviour of hydroxyapatite with different crystallinities, *Colloids Surf., B*, 74 (2009) 91–95.
- [22] D.L. Goloshchapov, V.M. Kashkarov, N.A. Rummyantseva, P.V. Seredinn, A.S. Lenshin, B.L. Agapov, E.P. Domashevskaya, Synthesis of nanocrystalline hydroxyapatite by precipitation using hen's egg shell, *Ceram. Int.*, 39 (2013) 4539–4549.
- [23] F. Granados-Correa, J. Vilchis-Granados, M. Jiménez-Reyes, L.A. Quiroz-Granados, Adsorption behaviour of La³⁺ and Eu³⁺ ions from aqueous solutions by hydroxyapatite: kinetic, isotherm and thermodynamic studies, *J. Chem.*, 2013 (2013) 1–9, doi: 10.1155/2013/751696.
- [24] C. Limei, H. Lihua, G. Xiaoyao, Z. Yakun, W. Yaoguang, W. Qin, D. Bin, Kinetic, isotherm and thermodynamic investigations of Cu²⁺ adsorption onto magnesium hydroxyapatite/ferro ferric oxide nanocomposites with easy magnetic separation assistance, *J. Mol. Liq.*, 198 (2014) 157–163.
- [25] R.R. Sheha, Sorption behavior of Zn²⁺ ions on synthesized hydroxyapatites, *J. Colloid Interface Sci.*, 310 (2007) 18–26.
- [26] R.M. Khaled, M.E. Zenab, A.S. Aida, *In vitro* properties of nanohydroxyapatite/chitosan biocomposites, *Ceram. Int.*, 37 (2011) 3265–3271.
- [27] R.J. Narayan, P.N. Kumta, C. Sfeir, D.-H. Lee, D. Olton, D.W. Choi, Nanostructured ceramics in medical devices: applications and prospects, *JOM*, 56 (2004) 38–43.
- [28] A. Krestou, A. Xenidis, D. Panias, Mechanism of aqueous uranium(VI) uptake by hydroxyapatite, *Miner. Eng.*, 17 (2004) 373–381.
- [29] S. Sugiyama, H. Matsumoto, H. Hayashi, J.B. Moffat, Sorption and ion exchange properties of barium hydroxyapatite with divalent cations, *Colloids Surf., A*, 169 (2000) 17–26.
- [30] A. Ruksudjarit, K. Pengpat, G. Rujijanagul, T. Tunkasiri, Synthesis and characterization of nanocrystalline hydroxyapatite from natural bovine bone, *Curr. Appl. Phys.*, 8 (2008) 270–272.
- [31] A. Siddharthan, T.S. Kumar, S.K. Seshadri, Synthesis and characterization of nanocrystalline apatites from eggshells at different Ca/P ratios, *Biomed. Mater.*, 4 (2009) 045010–045019.
- [32] E.M. Rivera, M. Araiza, W. Brostow, V.M. Castaño, J.R. Díaz-Estrada, R. Hernández, J.R. Rodríguez, Synthesis of hydroxyapatite from eggshells, *Mater. Lett.*, 41 (1999) 128–134.
- [33] R. Morsy, M. Elsayed, R. Krause-Rehberg, G. Dlubek, T. Elnimr, Positron annihilation spectroscopic study of hydrothermally synthesized fine nanoporous hydroxyapatite agglomerates, *J. Eur. Ceram. Soc.*, 30 (2010) 1897–1901.
- [34] G. Qian, W. Liu, L. Zheng, L. Liu, Facile synthesis of three dimensional porous hydroxyapatite using carboxymethylcellulose as a template, *Results Phys.*, 7 (2017) 1623–1627.
- [35] N.E. Tari, M.M.K. Motlagh, B. Sohrabi, Synthesis of hydroxyapatite particles in cationic mixed surfactants template, *Mater. Chem. Phys.*, 131 (2011) 132–135.
- [36] S. Mehdi, K. Alireza, H. Aydin, K. Semra, Preparation, characterization and application of a CTAB modified nanoclay for the adsorption of an herbicide from aqueous solutions: kinetic and equilibrium studies, *C. R. Chim.*, 18 (2015) 204–214.
- [37] Y. Park, Z. Sun, G.A. Ayoko, R.L. Frost, Removal of herbicides from aqueous solutions by modified forms of montmorillonite, *J. Colloid Interface Sci.*, 415 (2014) 127–132.
- [38] A. Cabrera, C. Trigo, L. Cox, R. Celis, M.C. Hermosin, J. Cornejo, W.C. Koskinen, Sorption of the herbicide aminocyclopyrachlor by cation-modified clay minerals, *Eur. J. Soil Sci.*, 63 (2012) 694–700.

- [39] A.F. Hassan, R. Hrdina, Department, Chitosan/nanohydroxyapatite composite based scallop shells as an efficient adsorbent for mercuric ions: Static and dynamic adsorption studies, *Int. J. Biol. Macromol.*, 109 (2018) 507–516.
- [40] Y. El-Nahal, Adsorption mechanism of chloroacetanilide herbicides to modified montmorillonite, *J. Environ. Sci. Health, Part B*, 38 (2003) 591–604.
- [41] B. Derkus, Y.E. Arslan, K.C. Emregul, E. Emregul, Enhancement of aptamer immobilization using egg shell-derived nano-sized spherical hydroxyapatite for thrombin detection in neuroclinic, *Talanta*, 158 (2016) 100–109.
- [42] Y. Azis, M. Adrian, C.D. Alfarisi, Khairat, R.M. Sri, Synthesis of hydroxyapatite nanoparticles from egg shells by sol-gel method, *IOP Conf. Ser.: Mater. Sci. Eng.*, 345 (2018) 1–6, doi: 10.1088/1757-899X/345/1/1012040.
- [43] A.F. Hassan, E. Hassan, A.M. Abdel-Mohsen, Adsorption and photocatalytic detoxification of diazinon using iron and nanotitania modified activated carbons, *J. Taiwan Inst. Chem. Eng.*, 75 (2017) 299–306.
- [44] L. Deng, Y. Su, S. Hua, X. Wang, X. Zhu, Sorption and desorption of lead(II) from wastewater by green algae *Cladophora fascicularis*, *J. Hazard. Mater.*, 143 (2007) 220–225.
- [45] S. Sasikumar, R. Vijayaraghavan, Low temperature synthesis of nanocrystalline hydroxyapatite from egg shells by combustion method, *Trends Biomater. Artif. Organs*, 19 (2006) 70–73.
- [46] P.H. Jai, J.S. Wook, Y.J. Kyu, K.B. Gil, L.S. Mok, Removal of heavy metals using waste egg shell, *J. Environ. Sci.*, 19 (2007) 1436–1441.
- [47] S. Meski, S. Ziani, H. Khireddine, S. Boudboub, S. Zaidi, Factorial design analysis for sorption of zinc on hydroxyapatite, *J. Hazard. Mater.*, 186 (2011) 1007–1017.
- [48] E.E. Berry, The structure and composition of some calcium-deficient apatites, *J. Inorg. Nucl. Chem.*, 29 (1967) 317–327.
- [49] Q. Hang, J. Xiao, Z. Dayong, Z. Beiwei, Q. Lei, M. Chun, O. Yihang, M. Yoshiyuki, Removal of heavy metals in aqueous solution using Antarctic Krill chitosan/hydroxyapatite composite, *Fibers Polym.*, 14 (2013) 1134–1140.
- [50] S. Rayanaud, E. Champion, D. Assollant, P. Thomas, Calcium phosphate apatites with variable Ca/P atomic ratio I synthesis, characterization and thermal stability of powders, *Biomaterials*, 23 (2002) 1065–1072.
- [51] T.A. Kuriakose, S.N. Kalkura, M. Palanichamy, D. Arivuoli, K. Dierks, G. Bocelli, Synthesis of stoichiometric nanocrystalline hydroxyapatite by ethanol based sol-gel technique at low temperature, *J. Cryst. Growth*, 263 (2004) 517–523.
- [52] I. Mobasherpour, M.S. Heshajin, A. Kazemzadeh, M. Zakeri, Synthesis of nanocrystalline hydroxyapatite by using precipitation method, *J. Alloys Compd.*, 430 (2007) 330–333.
- [53] G. Neha, A.K. Kushwaha, M.C. Chattopadhyaya, Adsorptive removal of Pb²⁺, Co²⁺ and Ni²⁺ by hydroxyapatite/chitosan composite from aqueous solution, *J. Taiwan Inst. Chem. Eng.*, 43 (2012) 125–131.
- [54] N.P. Katuwavila, A.D.L.C. Perera, S.R. Samarakoon, P. Soysa, V. Karunaratne, G.A.J. Amaratunga, D.N. Karunaratne, Chitosan-alginate nanoparticle system efficiently delivers doxorubicin to MCF-7 cells, *J. Nanomater.*, 2016 (2016) 1–12, doi: 10.1155/2016/3178904.
- [55] A.F. Hassan, A.M. Abdel-Mohsen, M.G.F. Moustafa, Comparative study of calcium alginate, activated carbon and their composite beads on methylene blue adsorption, *Carbohydr. Polym.*, 102 (2014) 192–198.
- [56] B.H. Hameed, A.A. Ahmad, Batch adsorption of methylene blue from aqueous solution by garlic peel, an agricultural waste biomass, *J. Hazard. Mater.*, 164 (2009) 870–875.
- [57] A.S. Taher, M.M. Ahmad, A.H. Mohamed, E.E. Bahgat, Development of nanohydroxyapatite/chitosan composite for cadmium ions removal in wastewater treatment, *J. Taiwan Inst. Chem. Eng.*, 45 (2014) 1571–1577.
- [58] C. Namasivayam, K. Ranganathan, Removal of Pb²⁺, Cd²⁺, Ni²⁺ and mixture of metal-ions by adsorption onto waste Fe³⁺, Cr³⁺ hydroxide and fixed-bed studies, *Environ. Technol.*, 16 (1995) 851–860.
- [59] Z. Aliakbaria, H. Younesia, A.A. Ghoreyshib, N. Bahramifara, A. Heidaric, Sewage sludge-based activated carbon: its application for hexavalent chromium from synthetic and electroplating wastewater in batch and fixed-bed column adsorption, *Desal. Water Treat.*, 93 (2017) 61–73.
- [60] K. Rathinam, M. Sankaran, Facile synthesis of cross linked-chitosan-grafted-poly aniline composite and its Cr⁶⁺ uptake studies, *Int. J. Biol. Macromol.*, 67 (2014) 210–219.
- [61] M. Akram, H.N. Bhatti, M. Iqbal, S. Noreen, S. Sadaf, Bio-composite efficiency for Cr(VI) adsorption: kinetic, equilibrium and thermodynamics studies, *J. Environ. Chem. Eng.*, 5 (2017) 400–411.
- [62] Z. Ren, G. Zhang, C.J. Paul, Adsorptive removal of arsenic from water by an iron-zirconium binary oxide adsorbent, *J. Colloid Interface Sci.*, 358 (2011) 230–237.
- [63] Q. Manzoor, A. Sajid, T. Hussain, M. Iqbal, M. Abbas, J. Nisar, Efficiency of immobilized *Zea mays* biomass for the adsorption of chromium from simulated media and tannery wastewater, *J. Mater. Res. Technol.*, 8 (2019) 75–86.
- [64] M.F. Elkady, M.M. Mahmoud, H.M. Abd-El-Rahman, Kinetic approach for cadmium sorption using microwave synthesized nanohydroxyapatite, *J. Non-Cryst. Solids*, 357 (2011) 1118–1129.
- [65] L. Xiaoli, Q. Yongxin, L. Yanfeng, Z. Yun, H. Xinghua, W. Yonghuan, Novel magnetic beads based on sodium alginate gel crosslinked by zirconium(IV) and their effective removal for Pb²⁺ in aqueous solutions by using a batch and continuous systems, *Bioresour. Technol.*, 142 (2013) 611–619.
- [66] A.F. Hassan, Enhanced adsorption of 2,4-dichlorophenoxyacetic acid from aqueous medium by graphene oxide/alginate composites, *Desal. Water Treat.*, 141 (2019) 187–196.
- [67] A.F. Hassan, R. Bulánek, Preparation and characterization of thiosemicarbazide functionalized graphene oxide as nano-adsorbent sheets for removal of lead cations, *Int. J. Environ. Sci. Technol.*, 16 (2019) 6207–6216.
- [68] A.M. Abdel-Mohsen, J. Jancar, L. Kalina, A.F. Hassan, Comparative study of chitosan and silk fibroin staple microfibrils on removal of chromium(VI): fabrication, kinetics and thermodynamic studies, *Carbohydr. Polym.*, 234 (2020) 115861–115872.
- [69] D. Yang, L. Li, B. Chen, S. Shi, J. Nie, G. Ma, Functionalized chitosan electrospun nanofiber membranes for heavy-metal removal, *Polymer*, 163 (2019) 74–85.
- [70] A. Maleki, B. Hayati, M. Naghizadeh, W.S. Joo, Adsorption of hexavalent chromium by metal organic frameworks from aqueous solution, *J. Ind. Eng. Chem.*, 28 (2015) 211–216.
- [71] J. Haniyeh, A. Paolo, C. Domenico, P. Antonio, Synthesis of amino-functionalized MIL-101 (Cr) MOF for hexavalent chromium adsorption from aqueous solutions, *Environ. Nanotechnol. Monit. Manage.*, 14 (2020) 100300–100310.
- [72] W. Zhifei, S. Qianqian, X. Jinbo, J. Husheng, X. Bingshe, L. Xuguang, Q. Li, Annealing temperature effect on 3D hierarchically porous NiO/Ni for removal of trace hexavalent chromium, *Mater. Chem. Phys.*, 240 (2020) 122140–122149.
- [73] C. Jung, J. Heo, J. Han, N. Her, S.J. Lee, J. Oh, J. Ryu, Y. Yoon, Hexavalent chromium removal by various adsorbents: powdered activated carbon, chitosan, and single/multi-walled carbon nanotubes, *Sep. Purif. Technol.*, 106 (2013) 63–71.
- [74] A.F. Hassan, F. Alafid, H. Radim, Preparation of melamine formaldehyde/nanozeolite Y composite based on nanosilica extracted from rice husks by sol-gel method: adsorption of lead(II) ion, *J. Sol-Gel Sci. Technol.*, 95 (2020) 211–222.

Supplementary information

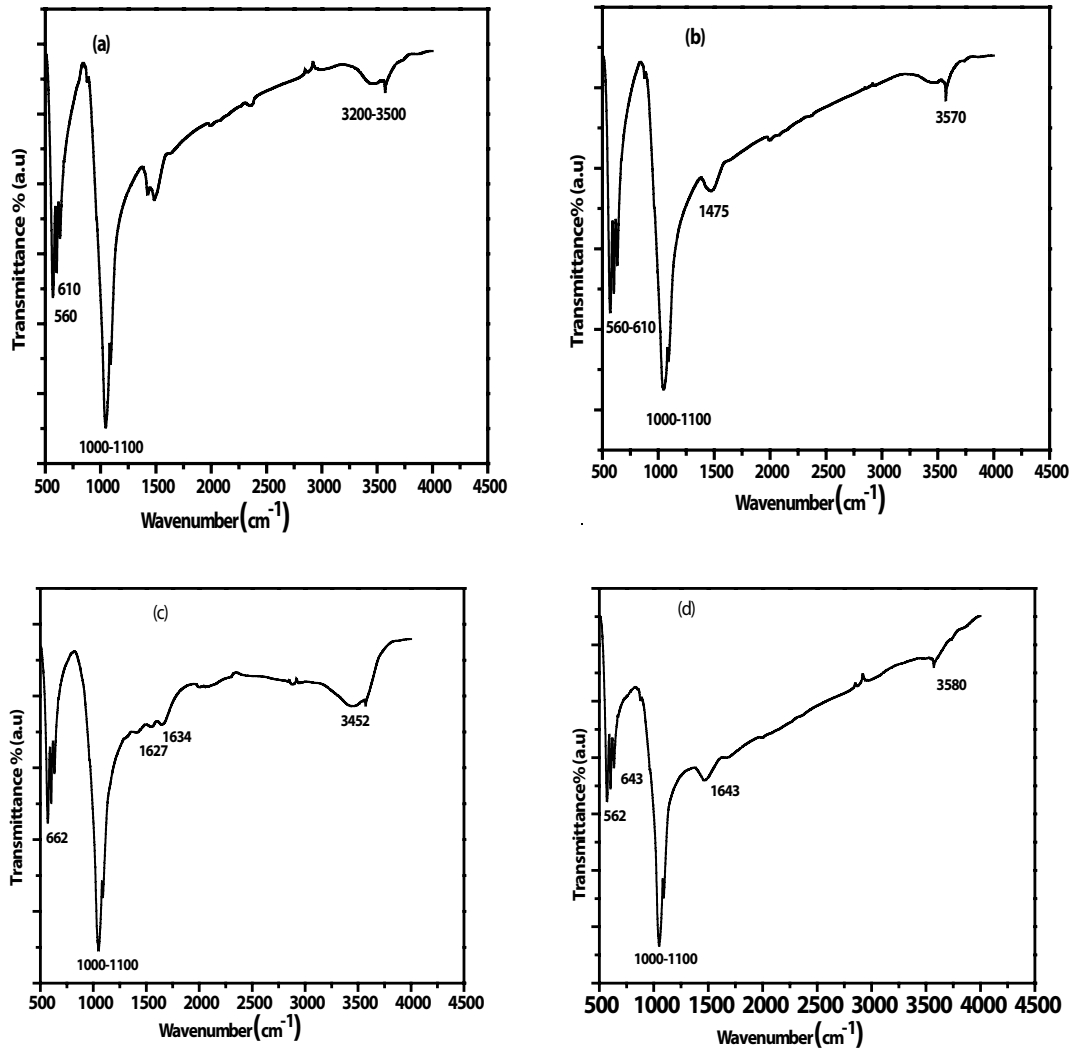


Fig. S1. FT-IR spectra for NP (a), NPB (b), NPS₁ (c), and NPS₂ (d), respectively.

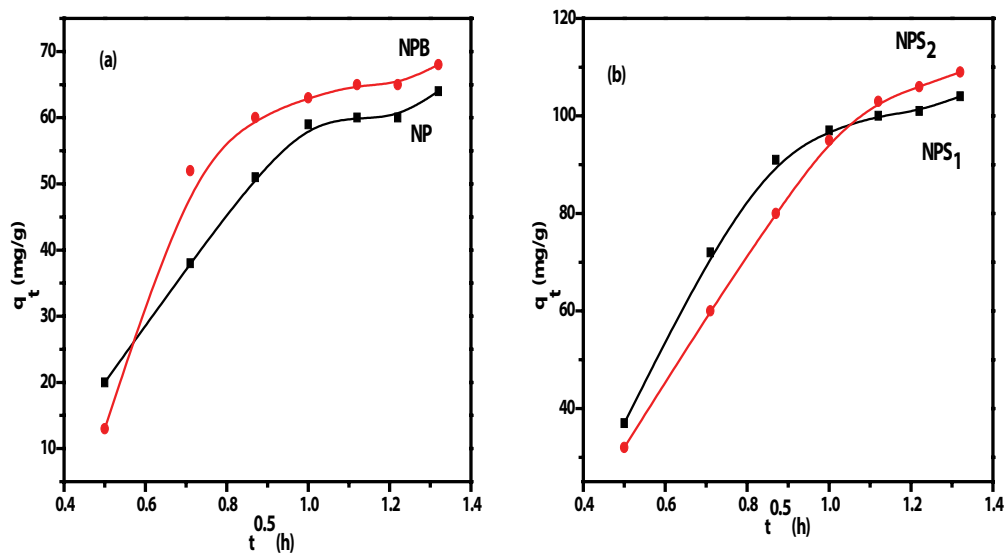


Fig. S2. Intraparticle diffusion plot for adsorption of chromium(VI) onto (a) NP, NPB, and (b) NPS₁, NPS₂ at 20°C.

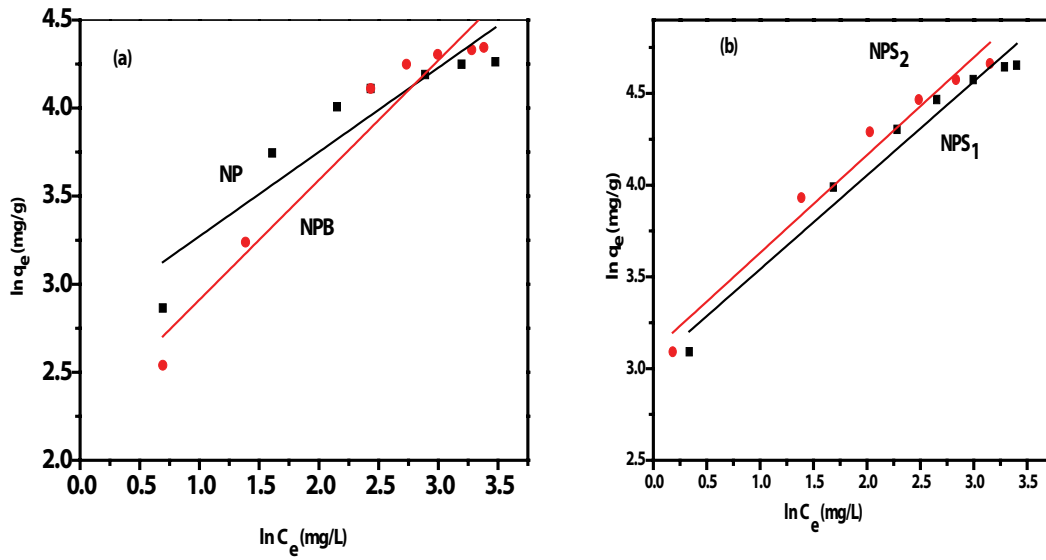


Fig. S3. Linear plot of Freundlich model for adsorption of chromium(VI) on (a) NP, NPB, and (b) NPS₁, NPS₂ at 20°C.

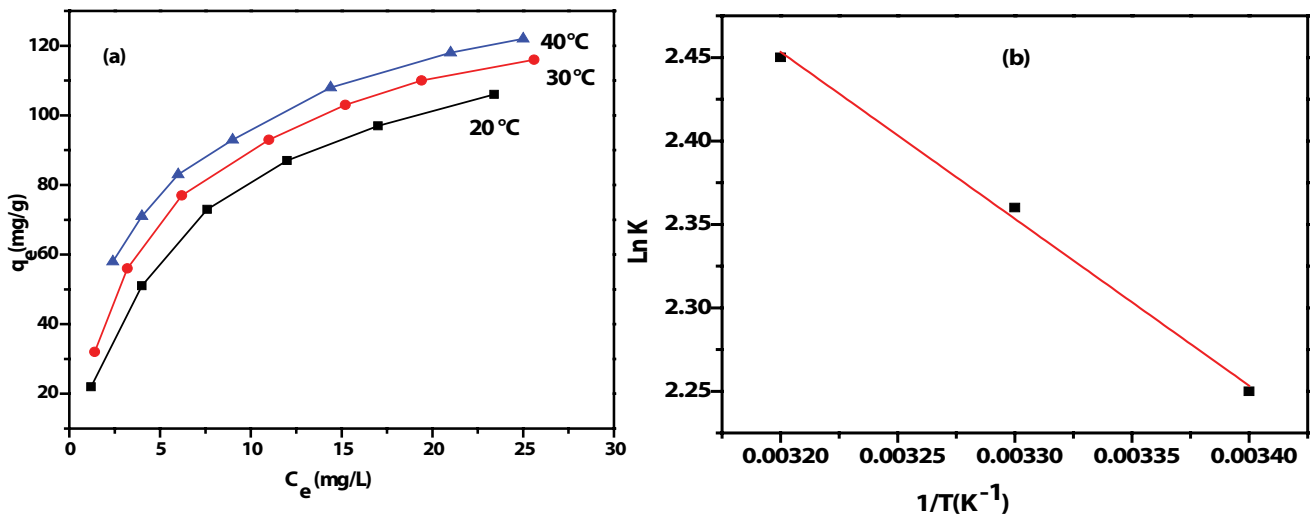


Fig. S4. Adsorption isotherms (a) and Van't Hoff plot for chromium(VI) (b) adsorption onto NPS₂ at 20°C, 30°C, and 40°C.